Author Manuscript

Author Manuscript

Author Manuscript

Author Manuscript

HHS Public Access

Author manuscript

Cancer Immunol Res. Author manuscript; available in PMC 2016 September 01.

Published in final edited form as:

Cancer Immunol Res. 2015 September ; 3(9): 1096–1107. doi:10.1158/2326-6066.CIR-14-0214.

Salmonella-Based Therapy Targeting Indoleamine 2,3-Dioxygenase Coupled with Enzymatic Depletion of Tumor Hyaluronan Induces Complete Regression of Aggressive Pancreatic Tumors

Edwin R. Manuel[1,†], **Jeremy Chen**[1], **Massimo D'Apuzzo**[2], **Melanie G. Lampa**[1], **Teodora I. Kaltcheva**[1], **Curtis B. Thompson**[3], **Thomas Ludwig**[4], **Vincent Chung**[5], and **Don J. Diamond**[1,†]

[1]Department of Experimental Therapeutics, Beckman Research Institute of City of Hope, Duarte, CA

[2]Department of Pathology, City of Hope Comprehensive Cancer Center, Duarte, CA

[3]Halozyme Therapeutics, Inc., San Diego, CA

[4]Department of Molecular Virology, Immunology and Medical Genetics, Ohio State University, Columbus, OH

[5]Department of Medical Oncology and Therapeutics Research, City of Hope Comprehensive Cancer Center, Duarte, CA

Abstract

Bacterial-based therapies are emerging as effective cancer treatments and hold promise for refractory neoplasms such as pancreatic ductal adenocarcinoma (PDAC), which has not shown significant improvement in therapy for over twenty-five years. Using a novel combination of shIDO-ST, a *Salmonella*-based therapy targeting the immunosuppressive molecule indoleamine 2,3-dioxygenase (IDO), with an enzyme, PEGPH20, which depletes extracellular matrix hyaluronan, we observed extended survival with frequent total regression of autochthonous and orthotopic PDAC tumors. This was associated with migration and accumulation of activated polymorphonuclear neutrophils (PMN) from spleens into tumors, which was not observed using a scrambled control (shScr-ST). Purified splenic PMNs from PEGPH20/shIDO-ST-treated mice exhibited significant IDO knockdown and were able to kill tumor targets *ex-vivo* through mechanisms involving FasL and serine proteases. In addition, $CD8^+$ T cells were observed to contribute to late control of pancreatic tumors. Collectively, our data demonstrate that entry of shIDO-ST and PMNs into otherwise impermeable desmoplastic tumors is facilitated by PEGPH20-mediated HA removal, further highlighting an important component of effective treatment for PDAC.

[†]**Correspondence:** E.R.M. or D.J.D: emanuel@coh.org; ddiamond@coh.org.

Potential Conflicts of Interest: Curtis B. Thompson is currently employed by Halozyme Therapeutics, Inc.

Author Manuscript Author Manuscript Author Manuscript Author Manuscript

Keywords

Salmonella; indoleamine 2,3-dioxygenase; cancer; neutrophils; PEGPH20

INTRODUCTION

Pancreatic ductal adenocarcinoma (PDAC) has an extremely poor prognosis due to the lack of early detection methods and substantial desmoplasia within the tumor stroma that prevents efficient drug delivery (1, 2). Currently, the approved drug combination of gemcitabine and nanoparticle albumin–bound paclitaxel (NAB, Abraxane®) for advanced PDAC has been shown to improve patient survival compared to standard gemcitabine monotherapy, yet it only extends survival an additional two to three months (3). One new focus to overcome chemoresistance in PDAC includes pre-treatment with agents that overcome aberrantly expressed components of the tumor stroma to significantly improve delivery of standard or novel therapeutics (4). For instance, the agent IPI-926 (5, 6) has recently been shown to inactivate the hedgehog protein Smoothened (Smo), resulting in decreased fibrosis and improved gemcitabine metabolism within PDAC tissue. Although no complete regression of tumors was observed, growth was significantly attenuated following combination treatment.

Hyaluronic acid (HA) is a component of PDAC stroma expressed at extremely high levels in the extracellular matrix (ECM) that forms a biophysical barrier to drug delivery. A promising agent known as PEGPH20, PEGylated human recombinant PH20 hyaluronidase, depletes HA in the ECM of PDAC tissue resulting in vascular decompression, enhanced drug delivery and stromal remodelling (7–9). Unlike other agents that target the tumor microenviroment (TME), PEGPH20-mediated HA removal was shown to generate microfenestrations and increase interendothelial junctional gaps, which ultimately promotes even greater macromolecular permeability within the tumor tissue. Of note, while combination treatment using PEGPH20 with gemcitabine inhibited PDAC growth and significantly prolonged survival in the *LSL-Kras$^{G12D/+}$; Trp53$^{R172H/+}$; Pdx1-Cre* (KPC) genetically engineered mouse model of pancreatic cancer, no complete regression of tumors was observed (7, 9).

Due to the relatively low efficacy of chemotherapy and the correspondingly high toxicity, novel strategies utilizing immunotherapy for treatment of PDAC are becoming more accepted and showing great promise (10, 11). For example, the combination of the GVAX Pancreas vaccine with the mesothelin-expressing *Listeria monocytogenes* (CRS-207) has been shown to extend survival in cyclophosphamide pre-treated patients that previously failed chemotherapeutic regimens (12). Although not yet tested specifically for PDAC, attenuated *Salmonella typhimurium* (ST) immunotherapy has been studied for decades for the treatment of solid tumors and has already been used in several clinical applications (10, 13, 14). Unlike in murine models, the use of ST alone in clinical trials of metastatic melanoma resulted in no significant changes in metastatic burden, but did show evidence of tumor colonization, indicating that ST could serve as a tumor-specific delivery vector (15).

Author Manuscript Author Manuscript Author Manuscript Author Manuscript

We have recently developed an immunotherapeutic agent known as shIDO-ST that has been shown to eradicate both tumor cells and associated stroma in a murine model of melanoma (16). Given the emerging success of bacterial-based therapies for treatment of solid tumors and the need for effective PDAC therapies, we tested the efficacy of shIDO-ST in combination with the HA-depleting agent PEGPH20 in orthotopic and autochthonous models of advanced pancreatic cancer (17). Our data suggest that simultaneously targeting tumor desmoplasia and immunosuppression significantly improves therapeutic delivery and enhances antitumor responses, ultimately resulting in greater control of PDAC.

MATERIALS AND METHODS

Animals and Cell Lines

C57BL/6 mice were obtained from breeding colonies housed at the City of Hope (COH) Animal Research Center and handled according to standard IACUC guidelines. The KPC PDAC cell line was derived from a KPC mouse generated from crossing the LSL-Kras-G12D, LSL-p53-R172H, and Pdx-1-Cre mice (NCI Frederick). Mice were backcrossed ≥10 times to achieve a predominantly C57BL/6 background. The tumor line was generated by the outgrowth method with minimal manipulation and passaging and then stored in liquid nitrogen. The KPC line expressing luciferase (KPC-luc) was generated using lentiviral transduction (Invitrogen). KPC-luc cells prior to implantation into C57BL/6 mice were passaged ≤ 2 times and maintained at ≤80% confluency in DMEM containing 10% FBS, 2mM L-glutamine and pen/strep.

Orthotopic Model and Therapy

Previously published methods (17) were used for orthotopic implantation of KPC-luc cells into the pancreas of C57BL/6 mice. Briefly, while anesthetized, a small incision was made in the skin and peritoneal lining and the pancreas externalized. Using a 27 gauge needle, approximately 5×10^5 KPC-luc cells in a volume of 50 uL PBS were injected into the body of the pancreas. Treatment of tumors occurred 13–14 days following orthotopic surgery, when tumors are 250–350 mm^3. Dosing schedule and concentrations are listed in Supplementary Fig. S2A. Endpoint for mice included signs of being moribund, ruffled fur, and visible protrusion of tumor by an unbiased animal technician. Endpoint also included estimated tumor sizes of ≥15 mm along the longest axis by palpation.

Immunohistochemistry (IHC) and Immunofluorescence (IF) Staining of Tissues

For IHC staining of HA, tumors from treated mice were fixed in 10% acid-formalin (Fisher Scientific) with 70% ethanol (18). Tumors were then sectioned and stained for HA using a biotinylated hyaluronan binding protein (Sigma) and visualized with a DAB kit (Vectastain). For IF, tumors were immediately flash frozen in optimal cutting temperature compound (Tissue-Tek) without prior fixation. Sections were fixed in cold acetone for 20 minutes, dried overnight, stained with primary antibody overnight at 4°C followed by incubation with fluorescently conjugated secondary antibody for 1 hour at room temperature. IHC and IF tissue sections were visualized using an Olympus AX70 microscope.

Author Manuscript Author Manuscript Author Manuscript Author Manuscript

Intravital Imaging (IVIS) and PMN tracking

Briefly, mice were injected intraperitoneally with 300 μg of D-luciferin (Gold Biotechnology) five minutes before imaging KPC-luc tumors using a Xenogen IVIS 100. For PMN tracking, a neutrophil-specific, near-infrared (NS-NIR) reagent (KeraFAST) was used (19). Briefly, treated mice were injected intravenously with 50 uL of a 20 uM working solution of NS-NIR. NS-NIR is a Cy7-labeled peptide, cFLFLFK-PEG_{76}-Cy7, specific for the formyl peptide receptor on PMNs (20). Mice were then imaged 45 min after NS-NIR injection using a Xenogen IVIS 100 or a Spectral Ami-X (Spectral Instruments Imaging) imager. Simultaneous imaging of tumors and PMNs was accomplished by injection of D-luciferin 5 minutes prior to imaging mice for detection of NS-NIR signal.

Cytotoxicity and Inhibition assays

Cytotoxicity against KPC-luc cells using crude splenocytes or purified splenic PMNs from treated mice was determined with a standard ^{51}Cr release assay (CRA) at different E:T ratios. Briefly, effectors used in the assay were derived from spleens of mice bearing KPC-luc tumors that had been treated with combinations of PBS, PEGPH20, shScr-ST, and shIDO-ST. Mice were sacrificed 96 hours post-ST treatment and crude splenocytes or purified PMNs were co-incubated with chromium-labeled KPC-luc targets (in triplicate) overnight (~16 hours). Parallel experiments were also done using culture supernatants from PMNs (16 hour cultures) or using 24-well transwell plates in which PMNs are held in 0.3 μm transwell baskets with ^{51}Cr-loaded tumor targets located at the bottom of the well. Radioactivity released into the supernatant was measured using a Cobra Quantum gamma counter (PerkinElmer). For inhibition experiments, purified PMNs from PBS-, PEGPH20/shScr-ST-, or PEGPH20/shIDO-ST-treated mice were used in CRA with targets as described above. Inhibitory agents to block PMN-specific production of ROS, NETs, FasL, and azurophilic proteases were added to the media to determine contribution to tumor target killing (21–24).

RESULTS

Combination of ShIDO-ST and PEGPH20 Controls Orthotopic KPC-luc Growth

To determine the efficacy of PEGPH20 with shIDO-ST (PEGPH20/shIDO-ST) in the orthotopic KPC-luc model (Supplementary Fig. S1), mice with established 14-day tumors of comparable size (~250–350 mm^3) were treated with combinations of PEGPH20, shIDO-ST, control scrambled ST (shScr-ST), gemcitabine (GEM) and NAB (Supplementary Fig. S2A; ref. 7, 25). Monotherapy with shIDO-ST, shScr-ST, NAB, GEM, and combination treatments with PEGPH20/shScr-ST, PEGPH20/GEM, NAB/GEM or PEGPH20/NAB/GEM resulted in no significant reduction in tumor growth or extension of survival (Fig. 1A, B and Supplementary Fig. S2B). Premature euthanization of treatment groups was predominantly due to extensive tumor progression and associated illness. The inability of PEGPH20/GEM and NAB/GEM to cause durable complete remission of tumors is consistent with what has been previously reported in GEMMs of PDAC (7, 25). However, the inability of these treatments to extend survival may be due to the aggressiveness of tumors generated through direct pancreatic implantation of cells that are derived from late-stage KPC neoplasms (17). These data suggest that the KPC-luc orthotopic model is as, or

Author Manuscript Author Manuscript Author Manuscript Author Manuscript

more, rigorous than current GEMMs and serves as a reasonable assessment for therapeutic efficacy.

In contrast, mice treated with the combination of PEGPH20/shIDO-ST showed a significant decrease in tumor burden with 100% of mice responding and approximately 30–60% of mice with no discernible evidence of tumors at two weeks post-treatment and extending to eight weeks following tumor implantation (Fig. 1A, B and Supplementary Fig. S3) ($p<0.01$, ANOVA). Supportive care of animals was not required following treatment and normal body weight maintenance was observed (Fig. 1C). Pathology in livers from mice treated with PEGPH20/shIDO-ST or PEGPH20/shScr-ST show portal and parenchymal inflammation with occasional foci of coagulative necrosis (Supplementary Fig. S4) with minimal inflammatory changes within kidney and pancreas which has been previously observed using VNP20009 (15). Overall size and weight of pancreata from PEGPH20/shIDO-ST-treated mice were not significantly different from that of normal, unmanipulated pancreata. In contrast to shIDO-ST alone or PEGPH20/shScr-ST treatment, these findings suggest that the combined effects of PEGPH20, IDO targeting, and ST are key for the efficacy of PEGPH20/shIDO-ST therapy.

PEGPH20/shIDO-ST Decreases Tumor Burden in an Autochthonous KPC model

To determine the efficacy of PEGPH20/shIDO-ST in an autochthonous setting, we implemented the use of the KPC-Brca1 model which is characterized by a more consistent and aggressive disease progression (26). Following PEGPH20/shIDO-ST treatment in KPC-Brca1 mice, we observed similar decreases in tumor burden and extension of survival found in the orthotopic model ($p<0.0001$) (Fig. 1D, E). Interestingly, we also found that in order to extend survival in PEGPH20/shIDO-ST-treated mice, pancreatic enzyme supplementation was required due to extensive ablation of the pancreas which is entirely comprised of tumor cells. In contrast, normal C57BL/6 mice orthotopically transplanted with KPC tumors did not require pancreatic enzyme supplementation as normal pancreatic tissue is still present after treatment with PEGPH20/shIDO-ST. Tumor growth and survival in mice treated with PEGPH20/shScr-ST, plus pancreatic enzyme supplement, were not significantly different from untreated KPC-Brca1 mice (data not shown) (26). These results confirm that PEGPH20/shIDO-ST treatment is effective in an aggressive autochthonous tumor setting and supports initial observations in the orthotopic model.

PEGPH20 Decompresses Intratumoral Vessels and Facilitates ST Tumor Entry

Previous studies using PEGPH20 in KPC GEMMs have shown significant depletion of HA in the extracellular matrix (ECM) of solid tumors, leading to increased vascularity and more efficient delivery of chemotherapy (7). Similarly, we observed significant colonization of orthotopic KPC tumors by shIDO-ST only with PEGPH20 pre-treatment (Supplementary Fig. S5A). Greater colonization of tumors was seen with Gr-1 depletion, re-emphasizing the role of PMNs in clearance of shIDO-ST in tumor tissue (Supplementary Fig. S5B; ref. 16). To assess the contribution of PEGPH20 in combination treatments, IHC and IF assays were performed on tumor tissues from PEGPH20-treated and untreated mice to evaluate HA depletion and vasculature. As shown in Fig. 2A, tumors from PEGPH20-treated mice were observed to be almost entirely devoid of HA 48 hours post-treatment compared to tumors of

Author Manuscript Author Manuscript Author Manuscript Author Manuscript

untreated mice. We confirmed the specificity of HA staining through depletion of HA in tumor sections treated with hyaluronidase or PEGPH20 (Supplementary Fig. S6). Thus, PEGPH20 effectively depletes HA in orthotopic PDAC tumors, which may significantly decrease tumor interstitial pressure.

To investigate whether PEGPH20 treatment leads to dilation of intratumoral vessels, sections from PEGPH20-treated and untreated tumors were stained for the endothelial marker CD31. Indeed, mice treated with PEGPH20 were observed to have a greater frequency of open intratumoral vessels compared to untreated control (Fig. 2B). Interestingly, although the mean luminal vessel area in PEGPH20-treated mice was found to be significantly increased ($p<0.01$, Student's t test) (Fig. 2C), we did not observe statistically significant increases in intratumoral vessel density (Fig. 2D), suggesting that any increases in tumor perfusion is likely due to the decompression of pre-existing vessels, which is consistent with previous observations (9).

Significant Influx of PMNs and ST into Orthotopic KPC Tumors using PEGPH20/shIDO-ST

Previous studies in our laboratory using shIDO-ST treatment in an aggressive B16F10 melanoma model revealed a large intratumoral influx of PMNs (16). To evaluate the involvement of PMNs in KPC-luc tumor regression using PEGPH20/shIDO-ST, we first studied the extent of PMN migration towards orthotopic tumors following treatment. Using a neutrophil-specific near infrared (NS-NIR) imaging peptide, which binds the formyl peptide receptor on PMNs and can be detected by IVIS (19, 20), we found that PMNs in an untreated, tumor-free mouse are predominantly localized to the spleen (Supplementary Fig. S7A). This is consistent with findings showing that PMN reside in the spleen as part of a large phagocyte system (27). Following treatment with shIDO-ST or shScr-ST alone, we observed that PMNs remained primarily in the spleens 24 to 72 hours post-treatment and did not observe any statistically significant recruitment into tumors (Supplementary Fig. S7B). However, noticeable increases in NS-NIR intensity could be observed in the spleens following shIDO-ST treatment, suggesting an activation of PMNs likely induced by the presence of shIDO-ST.

In contrast, combination treatment with PEGPH20/shIDO-ST, but not PEGPH20/shScr-ST, resulted in dramatic PMN tumor migration detected as early as 48 hours, with considerable tumor infiltration by 72 hours (Fig. 3A and Supplementary Fig. S7C). Coincident with PMN tumor infiltration at 48 hours and 72 hours, we also observed noticeable regression of KPC-luc tumors. When tumors were removed from mice 96 hours post-treatment and examined for the presence of PMNs using NS-NIR as a tracking agent injected into mice before biopsy, we observed a significant accumulation of PMNs specifically within the tumor of PEGPH20/shIDO-ST-treated mice as opposed to tumors of PEGPH20/shScr-ST-treated mice (Supplementary Fig. S8), providing further evidence that PMNs are indeed infiltrating into the tumor mass. Collectively, these data suggest that PEGPH20, prior to shIDO-ST treatment, enhances permeability of tumors through dilation of intratumoral vessels to facilitate the entry of PMNs.

Following PEGPH20/shIDO-ST treatment, it is hypothesized that significant shIDO-ST accumulation within tumor masses results in rapid and extensive movement of PMNs from

Author Manuscript Author Manuscript Author Manuscript Author Manuscript

the spleen into ST-colonized pancreatic tumors. We first examined tumors of treated mice for the presence cytokines involved in PMN recruitment. Indeed, quantitative PCR analysis of mRNA extracted from multiple tumors of PEGPH20/shIDO-ST-treated mice revealed a significant upregulation of chemotactic cytokines that included IL8 and MIP1α (Supplementary Fig. S9A). We also evaluated the expression of adhesion molecule ICAM-1 by IF and found comparable ICAM-1 distribution in treated versus untreated groups (Supplementary Fig. S9B). However, ICAM-1 was occasionally upregulated at the leading edges of PMN infiltration, which has been observed previously (28). We next assessed the extent and localization of intratumoral ST and PMNs by sectioning tumors from treated mice and performing immunofluorescence staining using antibodies specific to ST and PMN. In mice given shScr-ST or shIDO-ST alone (ST alone), we found no evidence of ST colonization or PMN infiltration (Fig. 3B), the latter of which is consistent with previous tracking experiments (Supplementary Fig. S7B). However, mice treated with PEGPH20/shIDO-ST showed significant influx of both shIDO-ST and PMNs primarily within the tumor core and, in some cases, on the outer perimeter of the tumor mass. These same observations were apparent in autochthonous tumors from KPC mice treated with PEGPH20/shIDO-ST (Supplementary Fig. S10). Under greater magnification we observed co-localization of shIDO-ST and PMNs suggesting phagocytosis of ST had occurred (Fig. 3C). Mice treated with PEGPH20/shScr-ST also demonstrated ST and PMN infiltration, however, not to the extent observed with PEGPH20/shIDO-ST treatment. Furthermore, PMN staining was observed to be centrally localized early during treatment with PEGPH20/shIDO-ST with no significant intermixing with tumor cells (Supplementary Fig. S11A, B).

Most interestingly, we observed DAPI-negative cells surrounded by PMNs present within the center of tumor masses of PEGPH20/shIDO-ST-treated mice, suggesting extensive tumor cell death caused by cytotoxic effects of infiltrating PMNs. To determine the extent of tumor killing by PMNs in treated tumors, we proceeded to stain for cleaved caspase-3 (CC3). In tumors of mice treated with PEGPH20/shIDO-ST (Fig. 3D), CC3 can be observed radiating outward from the perimeter of PMNs located immediately adjacent to DAPI-negative cells. Further analyses using western blot confirmed significant amounts of CC3 only in tumors of mice treated with PEGPH20/shIDO-ST compared to that of control groups (Supplementary Fig. S12). Overall, these data suggest that the procession of PMNs begins in the spleen and then migrates into the core of the tumor, disseminating cytotoxic effects outward to cause caspase-3 activation, tumor cell apoptosis, and ultimately leading to the generation of massive necrotic regions spanning the bulk of the tumor.

IDO knockdown in PMN, following shIDO-ST/PEGPH20 treatment, is associated with an activated antitumor (N1) polarized phenotype

PMN antitumor (N1-polarized) characteristics include enhanced production of reactive oxygen species (ROS), Fas-ligand-associated apoptosis, and immune recruitment and activation through production of chemokines and cytokines. Interestingly, the expression of IDO and downstream byproducts are known to reduce these processes and ultimately induce apoptosis in PMNs (29). The unique construction of shIDO-ST potentially allows for both IDO targeting and to act as a stimulus for PMN activation. In order to characterize the activation state of PMNs being recruited into the tumor, we isolated splenic PMNs from

Author Manuscript Author Manuscript Author Manuscript Author Manuscript

PEGPH20/shIDO-ST-treated mice for phenotypic and functional analyses. Since our prior tracking experiments suggested that tumor-infiltrating PMNs originated from the spleen, we sought to determine whether these PMNs were primed and capable of tumor killing. Purification of splenic PMNs by negative selection using magnetic bead separation, yielded populations of PMNs that were 85–95% pure as determined by FACS (Supplementary Fig. S13A). Splenic PMNs isolated 72 hours following PEGPH20/shIDO-ST treatment were observed to have a statistically significant IDO knockdown compared to PEGH20/shScr-ST-treated mice by quantitative RT-PCR (Fig. 4A).

To evaluate the activation state of isolated PMNs, we assessed intracellular ROS production by flow cytometric analysis using 2', 7'-dichlorofluorescein diacetate (DCFH-DA) (30). As shown in Fig. 4B, a significant amount of the ROS-cleaved product (DCF) is produced by PMNs in mice treated with PEGPH20/shIDO-ST compared to that in mice treated with PEGPH20/shScr-ST, suggesting a potential to induce apoptosis of tumor cells through oxidative-stress. We then investigated the expression of FasL in splenic PMNs isolated from PEGPH20/shIDO-ST-treated mice. Western blot analysis revealed upregulation of FasL in purified PMNs from PEGPH20/shIDO-ST-treated mice when compared to PEGPH20/shScr-ST-treated mice, suggesting that these PMNs have potential to induce tumor cell apoptosis through Fas-FasL signaling (Fig. 4C). We then evaluated levels of the serine proteases neutrophil elastase (NE) and cathepsin G (CG) in PMNs since they are a common defense against bacterial infection for clearance of intra- and extracellular microorganisms. We observed elevated levels of these proteases in PEPGH20/shIDO-ST-treated mice compared to PEGPH20/shScr-ST-treated mice. Additional immunofluorescence analyses in tumor sections of PEGPH20/shIDO-ST-treated mice confirmed the co-localization of FasL, CG, and NE with Gr-1$^+$ PMNs (Fig. 4D), suggesting that the activated PMN phenotype in spleens is retained after migrating into tumor tissue. FasL staining was localized more to the surface of PMNs, representing increased expression of transmembrane bound forms (31), whereas CG and NE were more diffuse, representing cytoplasmic localization or secretion of azurophilic granules (32). Taken together, these results demonstrate that PMNs observed in spleens or tumors of PEGPH20/shIDO-ST-treated mice are highly active in generating effector molecules that can contribute to tumor clearance.

Killing by PMN in PEGPH20/shIDO-ST-treated mice involves FasL and azurophilic proteases

Previously, we have shown that depletion of PMNs was sufficient to completely abrogate shIDO-ST function, whereas adaptive immune depletion had no significant effect on efficacy (16). Similarly, in this study we found that upon depletion of PMNs prior to PEGPH20/shIDO-ST treatment, we also observed complete abrogation of tumor growth control (Fig. 5A, Supplementary Fig. S13B and S14) ($p<0.01$, Student's t test), suggesting that PMNs are also essential mediators of anti-PDAC activity. Depletion of adaptive immune subsets did not significantly alter response rate to PEGPH20/shIDO-ST, however, CD8$^+$ T-cell depletion did increase late tumor rebound rate (Supplementary Fig. S14B), suggesting that CD8$^+$ T cells may play a role in late control of KPC tumors. We further tested the ability of purified splenic PMNs from PEGPH20/shIDO-ST-treated mice to kill KPC tumor targets using Cr^{51} killing assays. Target cells were either incubated directly with

Author Manuscript Author Manuscript Author Manuscript Author Manuscript

crude splenocytes or isolated splenic PMNs, or indirectly through the use of 16h culture media or transwells (33). Interestingly, purified PMNs from PEGPH20/shIDO-ST- or shIDO-ST-treated mice were sufficient to cause significant lysis of KPC target cells at an E:T ratio of 100:1 (Fig. 5B and Supplementary Fig. S15A), which was comparable to crude splenic preparations, suggesting that the bulk of tumor killing in crude preparations is mediated by PMNs. Significant tumor cell lysis only at high E:T ratios using purified PMNs also suggests that other factors in the serum or TME, such as complement or inflammatory cytokines, may be required to induce greater killing at lower E:T ratios. We also observed significant lysis of the 4T1 breast cancer cell line at an E:T of 100:1, but not of the B16F10 melanoma cell line, suggesting variable cross reactivity of PEGPH20/shIDO-ST-generated PMNs (Supplementary Fig. S15B and S15C). Culture media and transwell experiments using splenocytes or PMNs from PEGPH20/shIDO-ST-treated mice resulted in approximately 30–35% killing of targets ($p<0.01$, 1-way ANOVA), suggesting that soluble factors produced by PMNs also contribute to tumor killing.

Isolated PMNs were shown to kill tumor targets either when directly co-incubated or when using culture supernatant or transwells. Potential tumor-killing functions of PMNs can involve apoptotic-inducing processes such as the generation of neutrophil extracellular traps (NET), ROS, azurophilic proteases, and FasL. To test for these processes, we conducted *in vitro* inhibition assays under two conditions using 1) purified splenic PMNs (Fig. 5C), or 2) 16h culture media of purified splenic PMNs (Fig. 5D) from PEGPH20/shIDO-ST-treated mice to determine what mechanisms might be crucial for effective tumor-cell killing. In the case of NETs, previous studies have shown that histones contained within chromatin structures activate through toll-like receptors (TLR) to induce apoptosis of cells (34). In this case, heparin and PSA, which act to neutralize apoptotic function of histones (23), were unable to counteract tumor killing by PMNs under both conditions. DNAse I also had no effect, suggesting that extracellular chromatin itself does not contribute to tumor cell death.

We previously observed increased intracellular ROS production in PEGPH20/shIDO-ST-treated mice (Fig. 4C) and therefore sought to determine its role in tumor killing. Using the most common effective scavengers of ROS (catalase, thiourea, DMSO), we were unable to block killing of tumor cells *in vitro* (Fig. 5C), suggesting that ROS is not sufficiently released in high enough concentrations or ineffective for specifically killing PDAC tumor cells. Next, we sought to determine the role of serine proteases in tumor cell killing, which were previously observed to be elevated in PMNs (Fig. 4D). We tested protease inhibitors known to block NE, CG, and PR3 which included Sivelestat (S), chymostatin (C), and PMSF (P) (24). Sivelestat and chymostatin significantly inhibited killing under both conditions (10–15% inhibition, $p<0.01$) compared to PBS control, whereas PMSF provided far less inhibition (Fig.5C and 5D). Furthermore, combined inhibitors (S+C+P) increased inhibition up to 15–20%, (*n.s.*). The inability of the combined protease inhibitors to act additively may reflect broad specificity with overlapping functions.

To evaluate the role of FasL, we co-incubated effector PMNs with an anti-FasL blocking antibody (21) prior to incubating with targets. As shown in Fig. 5C, statistically significant (35–40%) inhibition of killing was observed compared to IgG control ($p<0.01$, 1-way ANOVA) under conditions in which PMNs were directly co-incubated with target cells.

Author Manuscript Author Manuscript Author Manuscript Author Manuscript

When antibody against soluble FasL (sFasL) was included in the culture media of PMNs, no significant inhibition of tumor killing was observed (Fig. 5D), suggesting that it does not contribute to KPC tumor cell apoptosis (35). Results from these studies indicate that other mechanisms may act synergistically with Fas/FasL to account for the total antitumor effect of PEGPH20/shIDO-ST. Collectively, these data suggest that PMNs induced by PEGPH20/shIDO-ST treatment are highly activated and induce tumor apoptosis through pathways involving serine proteases and membrane-associated FasL.

DISCUSSION

Despite advancements in the generation of effective stromal-targeting agents, combinatorial strategies are still limited by the use of ineffective therapies that are hampered by poor solubility, toxic side effects and limited antitumor potential (36). For example, gemcitabine, which is standard of care for PDAC, has a short *in vivo* half-life that significantly reduces its effectiveness (37). Currently, trials using nab-paclitaxel (NAB) with gemcitabine in patients with PDAC has shown median survival rates comparable to that of the more toxic FOLFIRINOX treatment (38). Although not yet tested specifically for PDAC, antibody therapies specific to the cytotoxic T-lymphocyte associated protein 4 (CTLA-4) and programmed cell death protein 1 (PD-1) have already shown great benefit towards tumor regression and survival in other solid tumor models (39). From these studies it is apparent that strategies to address immunosuppression and tumor specificity are actively being pursued. However, in the case of PDAC, an optimal treatment regimen will likely require the additional use of stromal-targeting agents to overcome desmoplasia and allow for optimal drug delivery.

Although we show that splenic PMNs migrate into PDAC tumors and kill tumor targets *ex vivo*, the detailed mechanisms to explain PMN migration are unknown. Movement of PMNs into tumors is likely influenced by transient circulation of ST through the extensive phagocyte system of the spleen, where it initially encounters and activates PMNs, which then migrate into tumor tissues where we and others have observed persistent ST colonization (Fig. 3B) (40). Induction of inflammatory cytokines as a result of ST tumor colonization (Supplementary Fig. S9A) acts as the necessary drivers for PMN recruitment. Additionally, the hypoxic centers of tumors provides an environment conducive for ST colonization and may explain the intratumoral staining pattern of shIDO-ST, PMN, and activated caspase-3 which originates centrally and radiates outward (41). The molecular mechanisms induced by shIDO-ST to trigger PMN migration could mirror those found in previous studies of sepsis that have revealed intravascular gradients of chemoattractants guiding PMNs precisely into infected areas (42). Specifically, bacterial antigens or damage-associated molecular pattern molecules within necrotic tissues resulted in the production of CXC-chemokines and endothelial adhesion molecules, such as ICAM-1 (Supplementary Fig. S9B), which facilitate PMN migration. In addition, recruitment could be augmented by the presence of intratumoral HA fragments produced by PEGPH20, which are known to act as stimuli for inflammatory mediators (43). Thus, determining the cascade of molecular events that contributes to the observed PMN migration pattern may guide additional strategies to encourage more comprehensive infiltration and clearance of tumor tissue.

Author Manuscript Author Manuscript Author Manuscript Author Manuscript

The dramatic differences in tumor regression, PMN activation and ST infiltration observed between shIDO-ST and shScr-ST treatments suggests that IDO-silencing plays an integral role in generating a focused, antitumor response. From our data, it is clear that shIDO-ST is localized within PMNs, which may account for significant IDO knockdown and acute hyperactivation since IDO is known to induce PMN apoptosis (29). Such an observation considerably increases the utility of IDO-silencing, not only for adaptive immunity (44), but also to enhance innate antitumor immunity, which has long been overlooked due to difficulties in inducing and focusing such cytotoxic responses (45). Determining if PEGPH20/shIDO-ST also induces late antitumor $CD8^+$ T-cell responses required for extended tumor regression (Supplementary Fig. S14B) would be an important aspect of the therapy and warrants further study. Previous studies of IDO function in infection models have also shown that its local upregulation, which leads to significant tryptophan depletion, results in decreased replication and improved clearance of microorganisms that depend on exogenous tryptophan (46). Thus, IDO-silencing may inadvertently augment PMN antitumor effects by allowing ST to replicate and persist in PDAC tissue. In support of this hypothesis, we have previously observed significantly increased intratumoral ST colonization in mice treated with shIDO-ST, which was not seen using shScr-ST (16).

PEGPH20 combined with chemotherapy has shown efficacy in autochthonous KPC models to extend survival (7, 9) and has been shown to be active in xenografts as a monotherapy (8), but was inactive alone in our orthotopic tumors. Presumably, the differences in the models, such as tumor stage, stromal composition, and immune infiltration may contribute to the variation in treatment efficacy (26, 47). In the orthotopic model, since implanted tumor cells originated from KPC mice with advanced metastatic PDAC, tumors are primarily composed of rapidly dividing tumor cells that have accrued numerous mutations and may already be prone to chemoresistance. Gemcitabine resistance in advanced metastatic PDAC has been associated with an epithelial-mesenchymal transition (EMT) phenotype and upregulated HIF1α and pERK expression (48). Additional studies to evaluate the extent of chemoresistance and the genetic basis in orthotopic KPC tumors could help to explain the inability of PEGPH20/GEM and NAB/GEM to extend survival in our model (7, 25). Ongoing studies using PEGPH20/shIDO-ST treatment in the autochthonous KPC model already show promising results (Fig. 1D, E) and suggest that PEGPH20/shIDO-ST is broadly efficacious even in stringent spontaneous PDAC models. The use of defined agents such as HA-depleting PEGPH20 and shIDO-ST, with continued success in preclinical autochthonous and xenograft models, should support further clinical development.

Supplementary Material

Refer to Web version on PubMed Central for supplementary material.

ACKNOWLEDGMENTS

Work was supported by NIH-R21-CA174306 (DJD), Tim Nesvig Foundation (DJD), and U54-CA163111 (T.L.). The COH Comprehensive Cancer Center is supported by P30-CA033572. We thank Gilbert Keller, H. Michael Shepard, and Daniel C. Maneval of Halozyme for PEGPH20 and experimental advice. We also acknowledge Jeffrey Molldrem at MD Anderson Cancer Center advice relating to PMN analyses.

Author Manuscript Author Manuscript Author Manuscript Author Manuscript

REFERENCES

1. Erkan M, Hausmann S, Michalski CW, Fingerle AA, Dobritz M, Kleeff J, et al. The role of stroma in pancreatic cancer: diagnostic and therapeutic implications. Nat Rev Gastroenterol Hepatol. 2012; 9:454–467. [PubMed: 22710569]
2. Lee JJ, Huang J, England CG, McNally LR, Frieboes HB. Predictive modeling of in vivo response to gemcitabine in pancreatic cancer. PLoS Comput Biol. 2013; 9:e1003231. [PubMed: 24068909]
3. Han H, Von Hoff DD. SnapShot: pancreatic cancer. Cancer Cell. 2013; 23:424-424.e1. [PubMed: 23518352]
4. Hamada S, Masamune A, Shimosegawa T. Novel therapeutic strategies targeting tumor-stromal interactions in pancreatic cancer. Front Physiol. 2013; 4:331. [PubMed: 24273517]
5. Lee MJ, Hatton BA, Villavicencio EH, Khanna PC, Friedman SD, Ditzler S, et al. Hedgehog pathway inhibitor saridegib (IPI-926) increases lifespan in a mouse medulloblastoma model. Proc Natl Acad Sci U S A. 2012; 109:7859–7864. [PubMed: 22550175]
6. Olive KP, Jacobetz MA, Davidson CJ, Gopinathan A, McIntyre D, Honess D, et al. Inhibition of Hedgehog signaling enhances delivery of chemotherapy in a mouse model of pancreatic cancer. Science. 2009; 324:1457–1461. [PubMed: 19460966]
7. Jacobetz MA, Chan DS, Neesse A, Bapiro TE, Cook N, Frese KK, et al. Hyaluronan impairs vascular function and drug delivery in a mouse model of pancreatic cancer. Gut. 2013; 62:112–120. [PubMed: 22466618]
8. Thompson CB, Shepard HM, O'Connor PM, Kadhim S, Jiang P, Osgood RJ, et al. Enzymatic depletion of tumor hyaluronan induces antitumor responses in preclinical animal models. Mol Cancer Ther. 2010; 9:3052–3064. [PubMed: 20978165]
9. Provenzano PP, Cuevas C, Chang AE, Goel VK, Von Hoff DD, Hingorani SR. Enzymatic targeting of the stroma ablates physical barriers to treatment of pancreatic ductal adenocarcinoma. Cancer Cell. 2012; 21:418–429. [PubMed: 22439937]
10. Vassaux G, Nitcheu J, Jezzard S, Lemoine NR. Bacterial gene therapy strategies. J Pathol. 2006; 208:290–298. [PubMed: 16362987]
11. Hardacre JM, Mulcahy M, Small W, Talamonti M, Obel J, Krishnamurthi S, et al. Addition of algenpantucel-L immunotherapy to standard adjuvant therapy for pancreatic cancer: a phase 2 study. J Gastrointest Surg. 2013; 17:94–100. discussion p.100–1. [PubMed: 23229886]
12. Lutz ER, Wu AA, Bigelow E, Sharma R, Mo G, Soares K, et al. Immunotherapy converts nonimmunogenic pancreatic tumors into immunogenic foci of immune regulation. Cancer Immunol Res. 2014; 2:616–631. [PubMed: 24942756]
13. Chorobik P, Czaplicki D, Ossysek K, Bereta J. Salmonella and cancer: from pathogens to therapeutics. Acta Biochim Pol. 2013; 60:285–297. [PubMed: 23828775]
14. Chen G, Wei DP, Jia LJ, Tang B, Shu L, Zhang K, et al. Oral delivery of tumor-targeting Salmonella exhibits promising therapeutic efficacy and low toxicity. Cancer Sci. 2009; 100:2437–2443. [PubMed: 19793349]
15. Toso JF, Gill VJ, Hwu P, Marincola FM, Restifo NP, Schwartzentruber DJ, et al. Phase I study of the intravenous administration of attenuated Salmonella typhimurium to patients with metastatic melanoma. J Clin Oncol. 2002; 20:142–152. [PubMed: 11773163]
16. Blache CA, Manuel ER, Kaltcheva TI, Wong AN, Ellenhorn JD, Blazar BR, et al. Systemic delivery of Salmonella typhimurium transformed with IDO shRNA enhances intratumoral vector colonization and suppresses tumor growth. Cancer Res. 2012; 72:6447–6456. [PubMed: 23090116]
17. Tseng WW, Winer D, Kenkel JA, Choi O, Shain AH, Pollack JR, et al. Development of an orthotopic model of invasive pancreatic cancer in an immunocompetent murine host. Clin Cancer Res. 2010; 16:3684–3695. [PubMed: 20534740]
18. Lin W, Shuster S, Maibach HI, Stern R. Patterns of hyaluronan staining are modified by fixation techniques. J Histochem Cytochem. 1997; 45:1157–1163. [PubMed: 9267476]
19. Xiao L, Zhang Y, Berr SS, Chordia MD, Pramoonjago P, Pu L, et al. A novel near-infrared fluorescence imaging probe for in vivo neutrophil tracking. Mol Imaging. 2012; 11:372–382. [PubMed: 22954181]

Author Manuscript Author Manuscript Author Manuscript Author Manuscript

20. Locke LW, Chordia MD, Zhang Y, Kundu B, Kennedy D, Landseadel J, et al. A novel neutrophil-specific PET imaging agent: cFLFLFK-PEG-64Cu. J Nuclear Med. 2009; 50:790–797.
21. Kayagaki N, Yamaguchi N, Nagao F, Matsuo S, Maeda H, Okumura K, et al. Polymorphism of murine Fas ligand that affects the biological activity. Proc Natl Acad Sci U S A. 1997; 94:3914–3919. [PubMed: 9108079]
22. Lichtenstein A, Seelig M, Berek J, Zighelboim J. Human neutrophil-mediated lysis of ovarian cancer cells. Blood. 1989; 74:805–809. [PubMed: 2546632]
23. Saffarzadeh M, Juenemann C, Queisser MA, Lochnit G, Barreto G, Galuska SP, et al. Neutrophil extracellular traps directly induce epithelial and endothelial cell death: a predominant role of histones. PloS One. 2012; 7:e32366. [PubMed: 22389696]
24. Standish AJ, Weiser JN. Human neutrophils kill Streptococcus pneumoniae via serine proteases. J Immunol. 2009; 183:2602–2609. [PubMed: 19620298]
25. Frese KK, Neesse A, Cook N, Bapiro TE, Lolkema MP, Jodrell DI, et al. nab-Paclitaxel potentiates gemcitabine activity by reducing cytidine deaminase levels in a mouse model of pancreatic cancer. Cancer Discov. 2012; 2:260–269. [PubMed: 22585996]
26. Shakya R, Gonda T, Quante M, Salas M, Kim S, Brooks J, et al. Hypomethylating therapy in an aggressive stroma-rich model of pancreatic carcinoma. Cancer Res. 2013; 73:885–896. [PubMed: 23204224]
27. Hume DA. Differentiation and heterogeneity in the mononuclear phagocyte system. Mucosal Immunol. 2008; 1:432–441. [PubMed: 19079210]
28. Roland CL, Dineen SP, Toombs JE, Carbon JG, Smith CW, Brekken RA, et al. Tumor-derived intercellular adhesion molecule-1 mediates tumor-associated leukocyte infiltration in orthotopic pancreatic xenografts. Exp Biol Med. 2010; 235:263–270.
29. Van der Sluijs K, Singh R, Dijkhuis A, Snoek M, Lutter R. Indoleamine-2,3-dioxygenase activity induces neutrophil apoptosis. Crit Care. 2011; 15:208. [PubMed: 21457506]
30. Himmelfarb J, Lazarus JM, Hakim R. Reactive oxygen species production by monocytes and polymorphonuclear leukocytes during dialysis. Am J Kidney Dis. 1991; 17:271–276. [PubMed: 1996568]
31. Kavurma MM, Khachigian LM. Signaling and transcriptional control of Fas ligand gene expression. Cell Death Differ. 2003; 10:36–44. [PubMed: 12655294]
32. Borregaard N, Cowland JB. Granules of the human neutrophilic polymorphonuclear leukocyte. Blood. 1997; 89:3503–3521. [PubMed: 9160655]
33. Serrao KL, Fortenberry JD, Owens ML, Harris FL, Brown LA. Neutrophils induce apoptosis of lung epithelial cells via release of soluble Fas ligand. Am J Physiol Lung Cell Mol Physiol. 2001; 280:L298–L305. [PubMed: 11159009]
34. Arazna M, Pruchniak MP, Zycinska K, Demkow U. Neutrophil extracellular trap in human diseases. Adv Exp Med Biol. 2013; 756:1–8. [PubMed: 22836612]
35. Hohlbaum AM, Moe S, Marshak-Rothstein A. Opposing effects of transmembrane and soluble Fas ligand expression on inflammation and tumor cell survival. J Exp Med. 2000; 191:1209–1220. [PubMed: 10748238]
36. Heinemann V, Quietzsch D, Gieseler F, Gonnermann M, Schonekas H, Rost A, et al. Randomized phase III trial of gemcitabine plus cisplatin compared with gemcitabine alone in advanced pancreatic cancer. J Clin Oncol. 2006; 24:3946–3952. [PubMed: 16921047]
37. Immordino ML, Brusa P, Rocco F, Arpicco S, Ceruti M, Cattel L. Preparation, characterization, cytotoxicity and pharmacokinetics of liposomes containing lipophilic gemcitabine prodrugs. J Control Release. 2004; 100(3):331–346. [PubMed: 15567500]
38. Thota R, Pauff JM, Berlin JD. Treatment of metastatic pancreatic adenocarcinoma: a review. Oncology. 2014; 28:70–74. [PubMed: 24683721]
39. Kvistborg P, Philips D, Kelderman S, Hageman L, Ottensmeier C, Joseph-Pietras D, et al. Anti-CTLA-4 therapy broadens the melanoma-reactive CD8+ T cell response. Sci Transl Med. 2014; 6:254ra128.
40. King I, Itterson M, Bermudes D. Tumor-targeted Salmonella typhimurium overexpressing cytosine deaminase: a novel, tumor-selective therapy. Methods Mol Biol. 2009; 542:649–659. [PubMed: 19565926]

Author Manuscript Author Manuscript Author Manuscript Author Manuscript

41. de Groot FM, Damen EW, Scheeren HW. Anticancer prodrugs for application in monotherapy: targeting hypoxia, tumor-associated enzymes, and receptors. Curr Med Chem. 2001; 8:1093–1122. [PubMed: 11472243]

42. McDonald B, Kubes P. Neutrophils and intravascular immunity in the liver during infection and sterile inflammation. Toxicol Pathol. 2012; 40:157–165. [PubMed: 22105645]

43. Black KE, Collins SL, Hagan RS, Hamblin MJ, Chan-Li Y, Hallowell RW, et al. Hyaluronan fragments induce IFNbeta via a novel TLR4-TRIF-TBK1-IRF3-dependent pathway. J Inflamm. 2013; 10:23.

44. Munn DH, Mellor AL. Indoleamine 2,3 dioxygenase and metabolic control of immune responses. Trends Immunol. 2013; 34:137–143. [PubMed: 23103127]

45. Sionov RV, Fridlender ZG, Granot Z. The Multifaceted Roles Neutrophils Play in the Tumor Microenvironment. Cancer Microenviron. 2014 Jun 4. [Epub ahead of print].

46. Carlin JM, Ozaki Y, Byrne GI, Brown RR, Borden EC. Interferons and indoleamine 2,3-dioxygenase: role in antimicrobial and antitumor effects. Experientia. 1989; 45:535–541. [PubMed: 2472288]

47. Clark CE, Hingorani SR, Mick R, Combs C, Tuveson DA, Vonderheide RH. Dynamics of the immune reaction to pancreatic cancer from inception to invasion. Cancer Res. 2007; 67:9518–9527. [PubMed: 17909062]

48. Zheng C, Jiao X, Jiang Y, Sun S. ERK1/2 activity contributes to gemcitabine resistance in pancreatic cancer cells. J Int Med Res. 2013; 41:300–306. [PubMed: 23569008]

Author Manuscript Author Manuscript Author Manuscript Author Manuscript

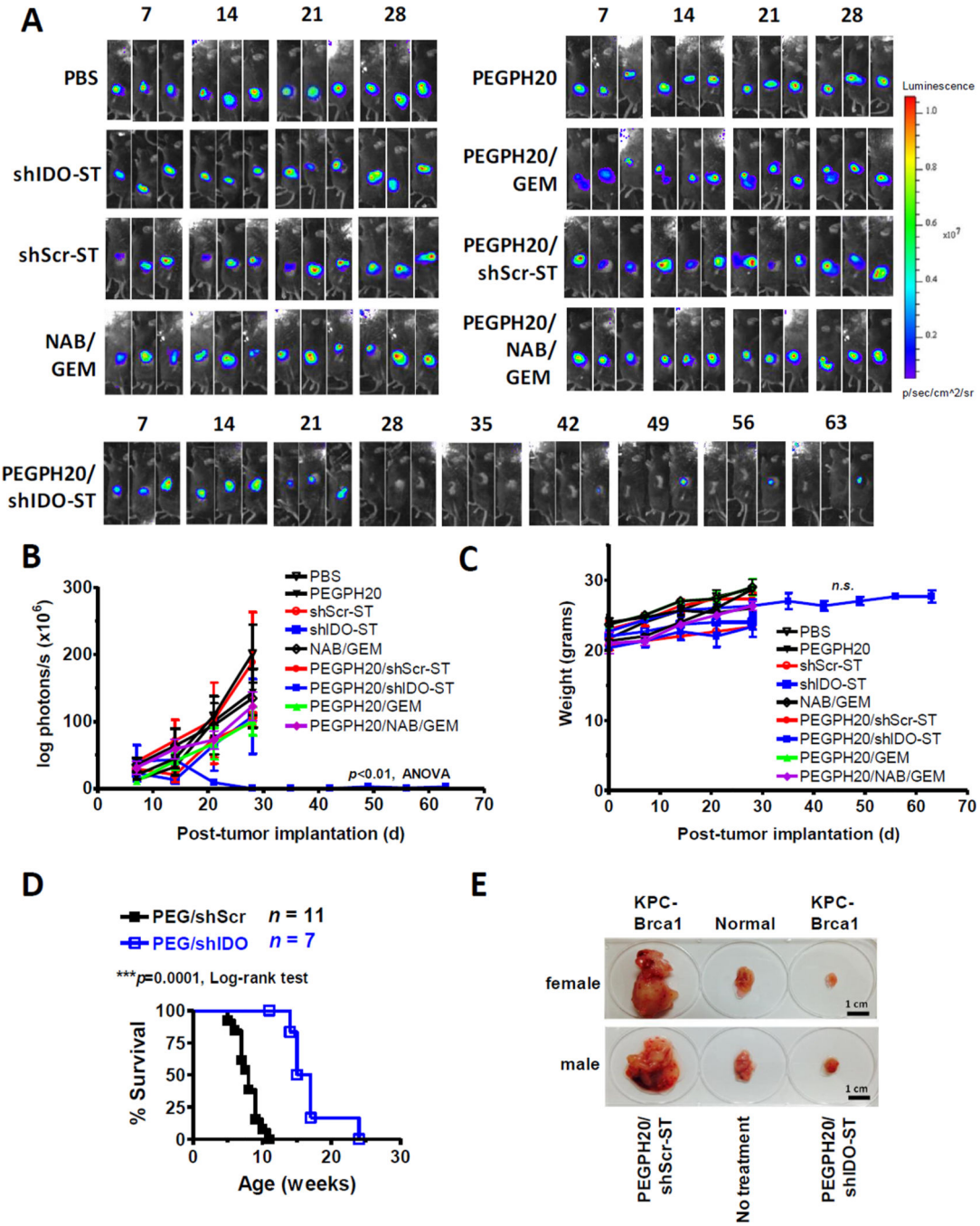

Figure 1. PEGPH20/shIDO-ST controls KPC tumor growth

(A) C57BL/6 mice were orthotopically implanted with $5x10^5$ KPC-luc cells on day 0 (numbers above images represent days post-implantation). Groups (n=3) were treated with indicated agents starting on day 14 and were imaged weekly by IVIS (heat map, false color) in the same order, until endpoint. Groups receiving combination treatments with PEGPH20 were given PEGPH20 on day 13. All images and data are representative of at least two separate experiments using identical treatment regimens. **(B)** Quantification of IVIS imaging using Living Image® software. **(C)** Mouse weights for orthotopically transplanted groups

Author Manuscript Author Manuscript Author Manuscript Author Manuscript

were measured prior to IVIS imaging to determine any changes in weight following administration of indicated treatments. **(D)** Survival curve of KPC-Brca1 mice treated with either PEGPH20/shIDO-ST or PEGPH20/shScr-ST at 7–8 weeks of age when palpable tumors are readily detected (approximately 600–800 mm^3). Treatment dose and schedule mirror those found in Supplementary Fig. 2A. **(E)** Autochthonous tumors excised from female and male KPC-Brca1 mice given indicated treatments. Normal pancreas indicates a litter mate negative for Pdx1-Cre recombinase (Cre-). Tumors were excised 2 weeks following initiation of treatment. $^{**}p<0.01$, 1-way ANOVA, *n.s.*, not significant. NAB, nanoparticle albumin–bound paclitaxel; GEM, gemcitabine.

Author Manuscript Author Manuscript Author Manuscript Author Manuscript

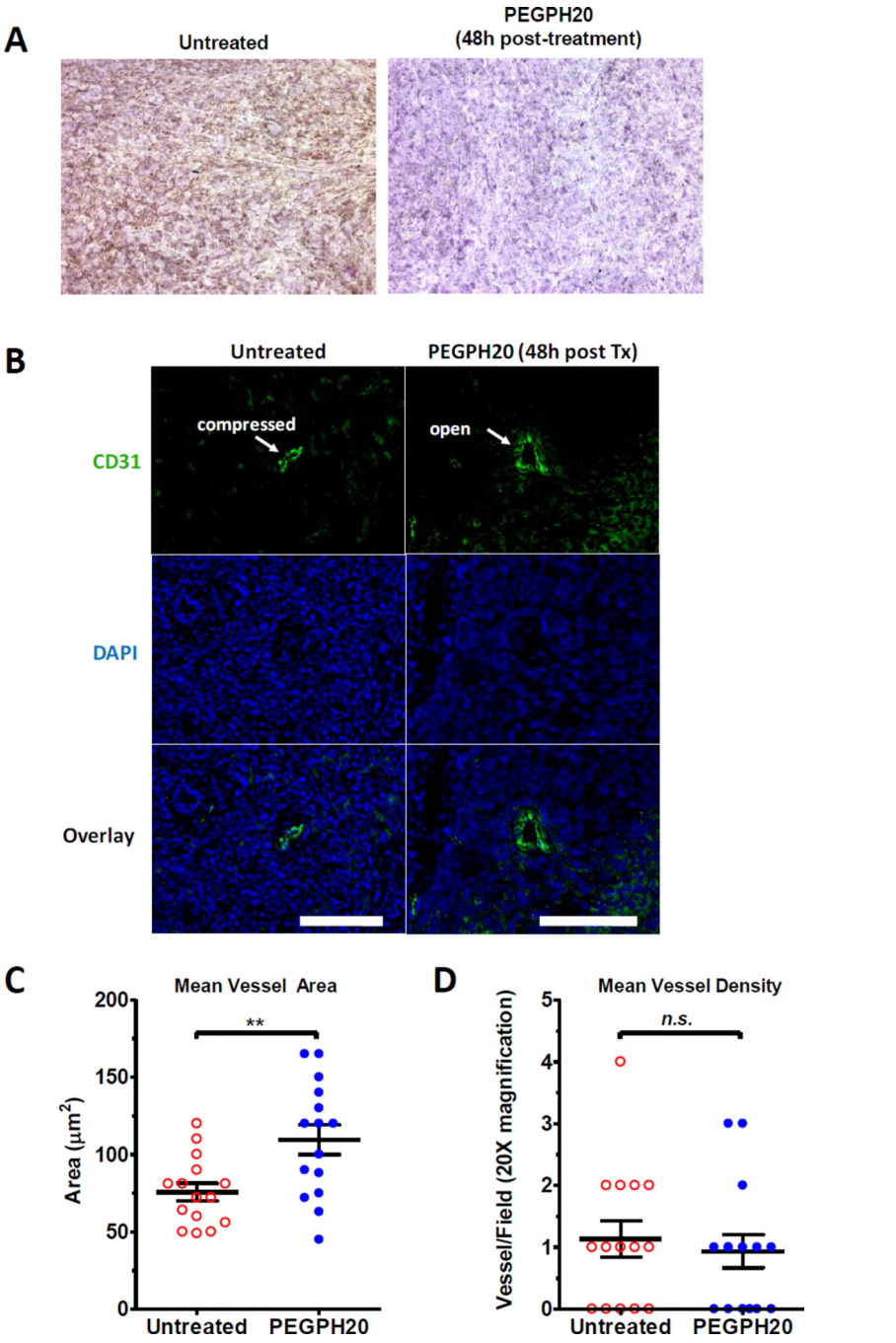

Figure 2. PEGPH20 depletes HA and decompresses intratumoral vessels

(A) Orthotopic tumors from untreated or treated with PEGPH20 on day 14 post-implantation were extracted, sectioned, and stained using biotin labeled HA-binding protein (HABP). DAB staining (brown) reveals HA deposits with counterstained nuclei (purple) using hematoxylin. Images are representative of at least two separate experiments using identical treatment regimens. **(B)** Sections of tumors from PEGPH20-treated and untreated mice were stained using a CD31 antibody and a FITC-conjugated secondary to detect vessels (green). DAPI staining was also performed to detect intact nuclei (blue). Closed vessels appear

Author Manuscript Author Manuscript Author Manuscript Author Manuscript

compressed, whereas open vessels are more ellipsoidal in shape. Images are representative of multiple tumor tissues treated with PEGPH20 or left untreated. Scale bars, 25 μm. **(C)** Mean vessel areas (μm^2) observed in tumor sections of mice treated with or without PEGPH20. Vessel area (n=5) were collected from tumor sections of multiple mice (n=3). **(D)** Mean vessel density observed in tumor sections of mice treated with or without PEGPH20. **p<0.01, Student's t test, *n.s.*, not significant. Vessel density was measured from 5 random fields of multiple mice (n=3).

Author Manuscript Author Manuscript Author Manuscript Author Manuscript

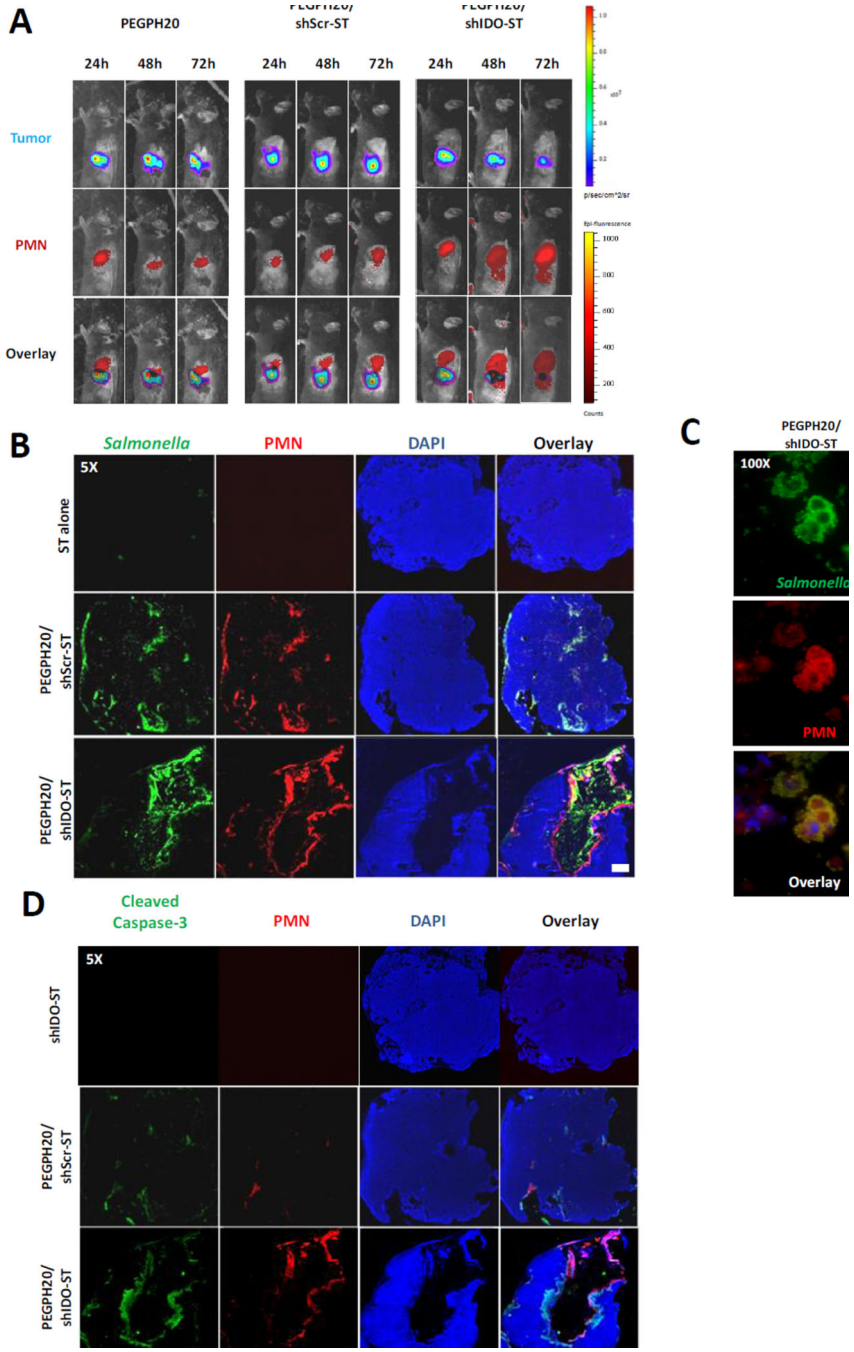

Figure 3. Greater influx of PMNs and ST using PEGPH20/shIDO-ST

(A) Mice treated with PEGPH20, PEGPH20/shScr-ST or PEGPH20/shIDO-ST were imaged at indicated time points following start of ST treatment. For each time point, mice were first injected with NS-NIR imaging agent specific to PMNs followed by injection with D-luciferin. Images are representative of at least two separate experiments using identical treatment regimens. **(B)** Sections of tumors from mice treated with ST alone, PEGPH20/ shScr-ST, or PEGPH20/shIDO-ST were stained for detection of ST, PMNs, and intact nuclei. ST alone represents mice treated with either shScr-ST or shIDO-ST. Scale bar, 1

Author Manuscript Author Manuscript Author Manuscript Author Manuscript

mm. **(C)** Areas of PEGPH20/shIDO-ST-treated tumors were magnified (100X) to visualize co-localization of ST and PMNs in PEGPH20/shIDO-ST-treated tumors. Scale bar, 5 um. **(D)** Sections of tumor from indicated treatment groups were stained for activated (cleaved) caspase-3, PMNs, and intact nuclei. Scale bar, 1 mm.

Author Manuscript Author Manuscript Author Manuscript Author Manuscript

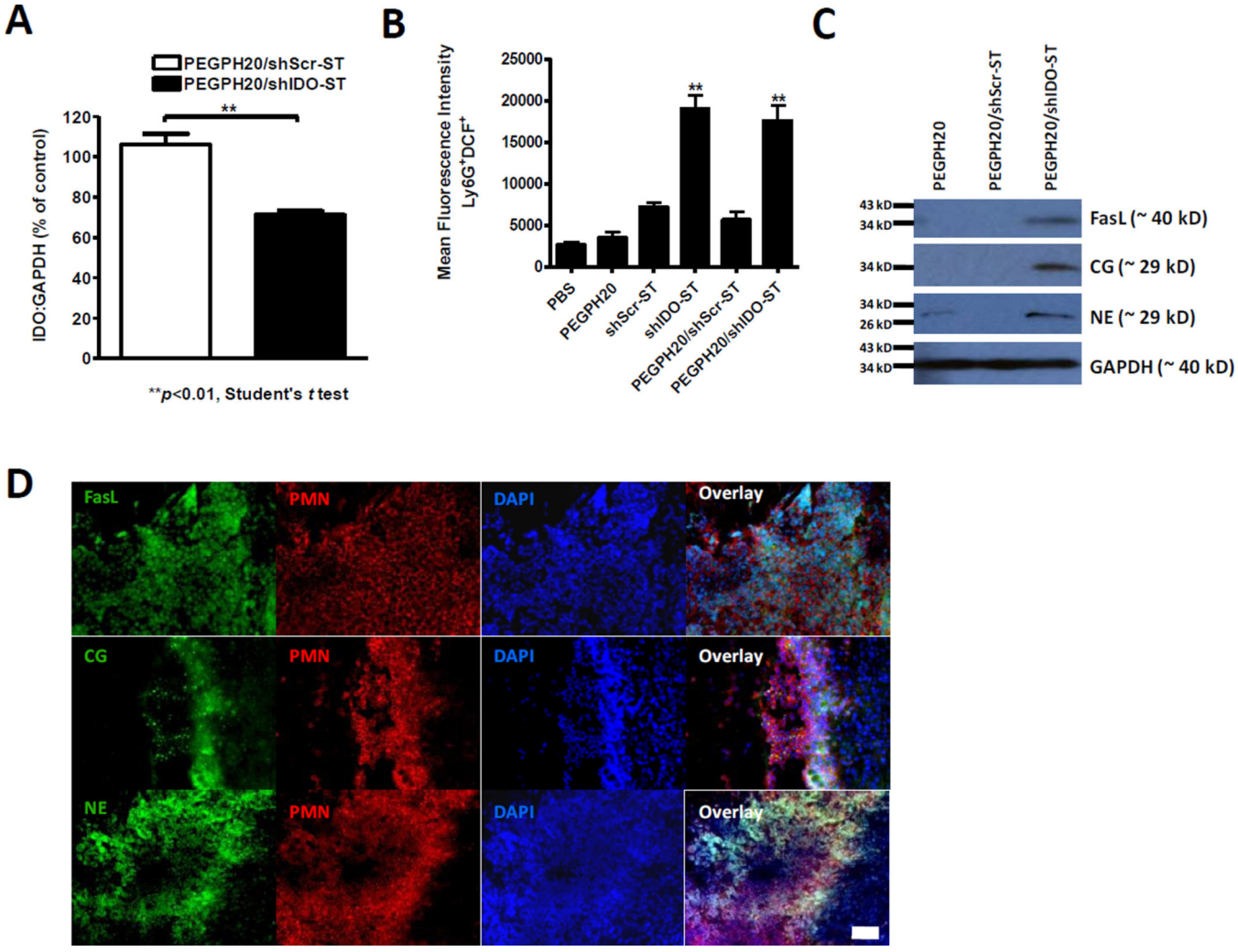

Figure 4. IDO knockdown and PMN phenotyping

(A) PMNs were isolated from spleens of PEGPH20/shScr-ST- and PEGPH20/shIDO-ST-treated mice through negative magnetic bead selection. IDO copies are normalized to the levels of IDO present in PMNs isolated from spleens of tumor-bearing mice treated with PEGPH20 alone. Quantitative RT-PCR experiments were done in triplicates and are representative of at least two separate experiments using identical treatment regimens. **(B)** Mean fluorescence intensity (MFI) of $Ly6G^{+}DCF^{+}$ cells present in total $CD45^{+}$ cells from spleens of indicated treatment groups (n=6). Treatment groups were compared to shScr-ST-treated mice for 1-way ANOVA analysis, $^{**}p<0.01$. Scale bar, 250 um. **(C)** Western blot analysis of FasL, cathepsin G (CG), and neutrophil elastase (NE) from PMNs isolated from tumors of treated mice. GAPDH is used as a loading control. **(D)** Co-immunofluorescence staining of PMNs and FasL, CG, or NE in tumors from PEGPH20/shIDO-ST-treated mice.

Author Manuscript Author Manuscript Author Manuscript Author Manuscript

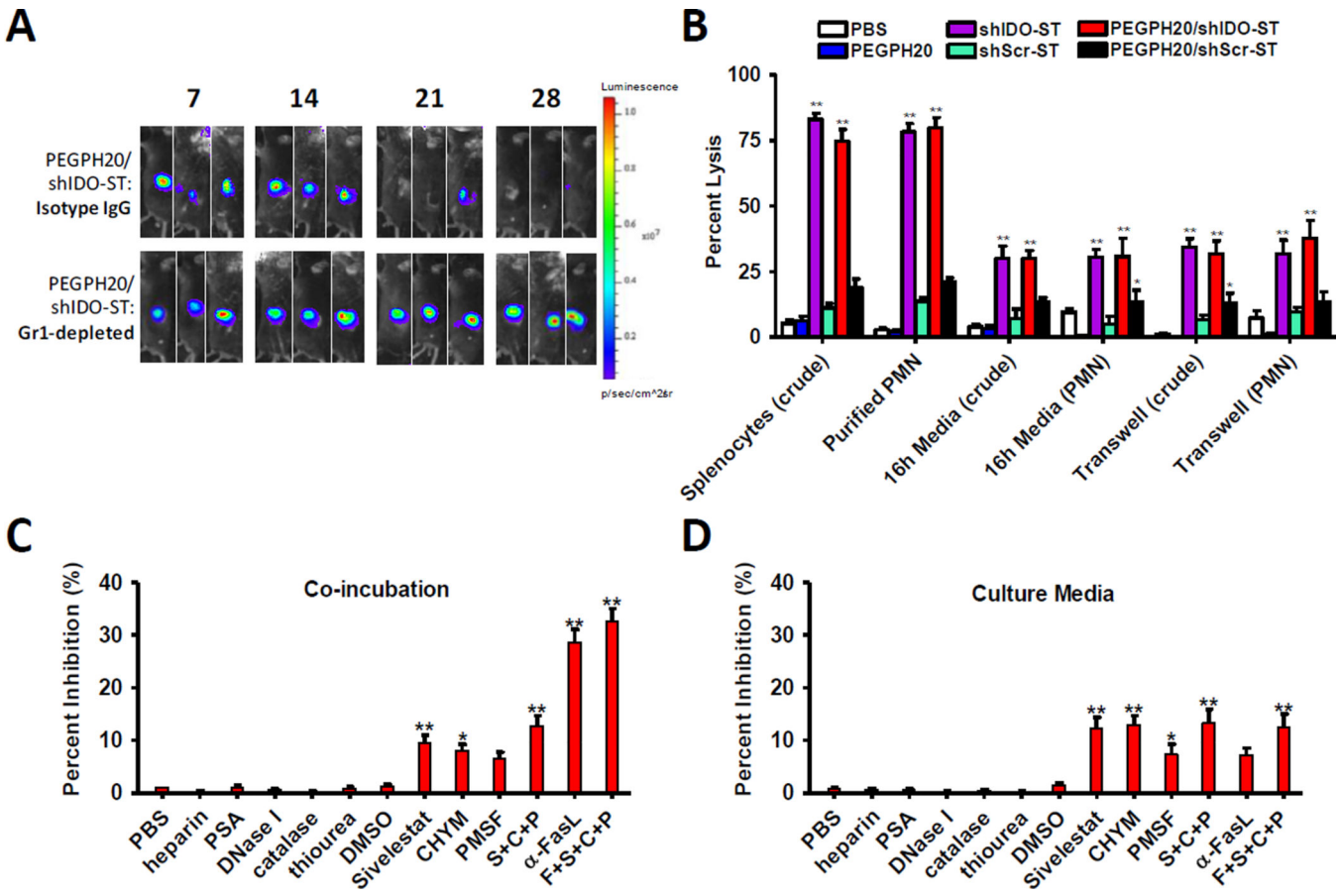

Figure 5. PEGPH20/shIDO-ST mechanism of tumor control through PMN is primarily dependent on FasL and azurophilic proteases

(A) Tumor-bearing mice (*n*=3) were treated with Gr-1-depleting antibody (60 ug/injection), or isotype control, on day 12 post-tumor implantation with maintenance depletions every 3 days. Mice were then given PEGPH20/shIDO-ST treatment following the normal dose and schedule. Images are representative of at least two separate experiments using identical treatment regimens. **(B)** Splenocytes or purified PMNs from treated mouse groups were used in a ^{51}Cr cytotoxicity assay. Targets were co-incubated directly with effectors, 16h culture supernatants, or indirectly with effectors. Percent lysis within each condition was compared to shScr-ST-treated group by 1-way ANOVA analysis. **(C)** Inhibitors of NET, ROS, protease, or FasL-mediated cell apoptosis were co-incubated with targets and purified PMNs from PEGPH20/shIDO-ST-treated mice. All inhibitors were compared to PBS control or IgG for α-FasL, for ANOVA analysis. **(D)** Inhibitors of NET-, ROS-, protease-, or FasL-mediated cell apoptosis were co-incubated with cultured media of purified PMNs from PEGPH20/shIDO-ST-treated mice. All inhibitors were compared to PBS control or IgG for α-FasL, for 1-way ANOVA analysis. *p<0.05, **p<0.01.